Macromolecules

ARTICLE

pubs.acs.org/Macromolecules

Conformations of Amphiphilic Polyelectrolyte Stars with Diblock Copolymer Arms

Alexey A. Polotsky,[†] Tatiana M. Birshtein,[†] Mohamed Daoud,[‡] and Oleg V. Borisov*[,§,†]

[†]Institute of Macromolecular Compounds, Russian Academy of Sciences, 31 Bolshoy pr., 199004 St. Petersburg, Russia

[‡]Service de Physique de l'Etat Condensé, CEA Saclay, 91191 Gif-sur-Yvette Cedex, France

[§]Institut Pluridisciplinaire de Recherche sur l' Environnement et les Matériaux, UMR 5254 CNRS/UPPA, Pau, France

ABSTRACT: We consider conformations and intramolecular conformational transitions in amphiphilic starlike polymers formed by diblock copolymer arms with inner hydrophobic and outer polyelectrolyte blocks. A combination of an analytical mean-field theory with the assumption free numerical self-consistent field (SCF) modeling approach is applied. It is demonstrated that unimolecular micelles with collapsed hydrophobic cores and swollen polyelectrolyte coronae are formed in dilute aqueous solutions at high ionic strength or/and low degree of ionization of the outer hydrophilic block. An intramolecular conformational transition related to the unfolding of the hydrophobic core of the unimolecular micelles can be triggered by a decrease in the ionic strength of the solution or/and increase in the degree of ionization of the coronal blocks. In the stars with large number of diblock copolymer arms the transition between conformations with collapsed or stretched core-forming blocks occurs continuously by progressive unfolding of the core domain. By contrast, in the stars with relatively small number of arms the continuous unfolding of the core is interrupted by an abrupt unravelling transition. A detailed SCF analysis indicates that under both unfolding scenarios the arms of the star are extended fairly equally; i.e., no intramolecular disproportionation occurs.

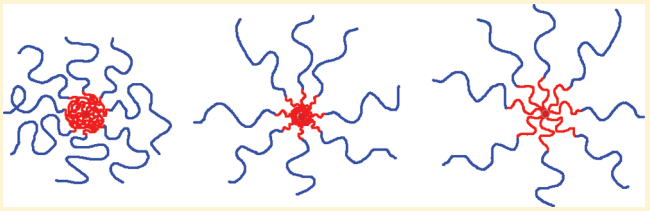

INTRODUCTION

Micelles of amphiphilic block copolymers attract a lot of attention in recent years because of their potential use in applications including emulsion stabilization, viscosity regulation, biomedical applications, and nanotechnology.[1] One of the most interesting and promising fields of application of amphiphilic block copolymers is their use for controlled drug delivery. Many effective drug candidates have limited solubility and stability and can be even rather dangerous because of their toxicity. To avoid these transport problems, drug delivery systems on the basis of amphiphilic block copolymer micelles with hydrophobic core and water-soluble corona have been proposed.[2,3] In this case the core encapsulates a drug whereas the hydrophilic corona makes this system soluble, protects from aggregation, and even makes it selective with respect to the pore size, thus allowing it to penetrate only into tumor tissues.[4] By attaching a specific terminal group to the corona chain, biocompatibility and/or selectivity can be further enhanced. Upon reaching the target compartment, a proper release of the drug molecules from the micelle should follow in response to the change in the surrounding conditions. The latter in most cases is the pH shift. For example, if the cellular uptake occurs via endocytosis,[4,5] the pH changes from its physiological value pH 7.4 to sufficiently lower value pH 4−5 in lysosome. Drug release can occur via dissociation of the block copolymer micelle, cleavage of the corona chains, or by conformational changes in the core itself. The use of starlike $(AB)_p$ block copolymers with hydrophobic inner B blocks and hydrophilic outer A blocks which form in solution the so-called unimolecular micelles (Figure 1a) has definite advantages over the self-assembled AB diblock copolymer micelles. Unimolecular micelles are more stable with respect to shear force, temperature, and pressure (often used for sterilization) than the block copolymers aggregate and, therefore, are more suitable for the noncovalent encapsulation of guest molecules. Moreover, formation of the unimolecular micelles does not imply cooperative intermolecular association; that is, there is no CMC. Therefore, vector systems based on the unimolecular micelles can be used at arbitrary low concentration. Another advantage is the prescribed "aggregation number", i.e. the number of star arms p and, thus, a better control of the micelle size.This property is also very important for application of $(AB)_p$ unimolecular micelles as nanoreactors for synthesis of metal nanoparticles. At present, methods of synthesis of $(AB)_p$ stars are quite well developed,[6] and stars with different chemical nature of arm blocks solvable in water and organic solvents were obtained. They were successfully used for synthesis of gold[7] and platinum[8] nanoparticles. First steps in the creation of drug delivery systems on the basis of $(AB)_p$ unimolecular micelles were also made.[4] The final and, therefore, crucial stage in the successful work of a drug delivery system is the drug release when it reaches the target compartment. Drug release can occur, as it was mentioned above, via degradation

Received: July 25, 2011
Revised: September 27, 2011
Published: October 25, 2011

of the core or of the micelle as a whole, but it may be useful to keep the $(AB)_p$ star intact (for example, if the core polymer itself cannot be safely removed from the body). This means that the drug release should be made through unfolding of the globular core (Figure 1b,c). The driving force of this unfolding transition may be an increase of the repulsive interactions in the corona (or a decrease in attractive interactions in the core or both together) induced by variation of the environmental conditions. The corona of the $(AB)_p$ unimolecular micelle can be modeled as a convex spherical polymer brush grafted onto the B-core and immersed into a good solvent. This system was the subject of intensive theoretical studies in the past two decades beginning at the classical works of Daoud and Cotton,[9] Zhulina,[10,11] and Birshtein and Zhulina.[12] In more recent work of Zhulina, Birshtein, and Borisov[13] the Daoud−Cotton model have been revised, generalized, and extended on the convex polyelectrolyte brush. It should be noted that these approaches employed the so-called "fixed ends" (or equal stretching) approximation, consisting in the assumption that the free ends of the grafted chains are localized at the edge of the brush; hence, all chains are equally, although not uniformly, stretched. For planar polymer brushes this approximation is often referred to as Alexander−de Gennes approximation.[14,15] The collapsed core of the unimolecular micelle can be also considered as a spherical polymer brush grafted to a small sphere with the free ends fixed at the outer boundary of the brush (hence, the core fits well to the Alexander−de Gennes approximation). Coil−globule transition in the star-shaped polymer in poor solvent was studied by Zhulina et al.[16] using the scaling approach. It was demonstrated that under poor solvent conditions the intramolecular concentration profile consists of two parts: a denser inner (central) zone is due to tethering of the star arms to the central point; here the polymer concentration decays inversely proportional to the distance from the star center. In the rest of the star the concentration is constant and is equal to the characteristic concentration of the collapsed polymer globule. The core-forming B-blocks of the amphiphilic star copolymer are subjected to the radial pulling force exerted by crowded coronal blocks. When this force exceeds a certain critical threshold, it may induce unraveling of the collapsed core and stretching of the B-blocks in the radial direction. In particular, the long-range Coulomb interactions between ionic (polyelectrolyte) A-blocks under low ionic strength conditions may be strong enough to provoke such kind of conformational transition. In ref 17, conformational characteristics of amplhiphilic $(AB)_5$ star (with block lengths $N_A = 80$, $N_B = 20$, and fraction of charged units in the A block $\alpha_b = 0.5$) as functions of ionic strength were studied by means of numerical self-consistent field modeling. It was shown that at high salt concentrations all B-blocks are not extended by charged A-blocks and collapse in the core while at low salt concentrations the B-blocks are strongly stretched due the corona pulling force. Monte Carlo simulation of $(AB)_p$ stars were performed by Nelson et al.,[18] who considered not only the star with solvophobic core and solvophilic corona but also the opposite interesting case (solvophilic inner + solvophobic outer blocks), paying more attention to the latter one. In these simulations, solvent was athermal for the solvophilic block, and the Flory parameter for the outer block was varied. It was found that the stars which have the innter solvophilic block can undergo a dramatic conformational change in which the outer solvophobic blocks aggregate into one or more compact globules. This aggregation transition is accompanied by a significant change in the size of the polymer as measured by the radius of gyration. In the case of stars in which the inner blocks are solvophobic and the outer blocks are solvophilic like in our study, no such transition was found.

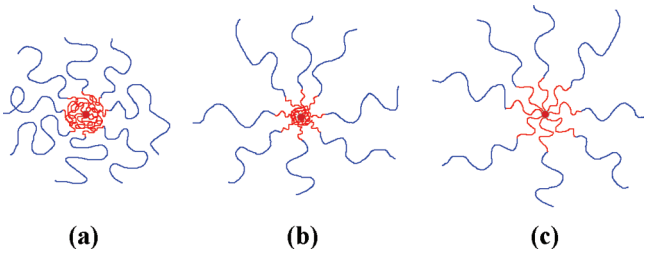

Figure 1. $(AB)_p$ core−shell star copolymer with collapsed (a), partially unfolded (b), and completely unfolded (c) core.

The aim of the present work is to study equilibrium conformations of the amphiphilic $(AB)_p$ star block copolymers with hydrophobic B-blocks and strongly dissociating (quenched) polyelectrolyte A-blocks. We are particularly interested in the analysis of the stimuli-induced conformational (unfolding) transition in the $(AB)_p$ star triggered by the change in the ionic strength of the solution or/and degree of ionization of the A-blocks, which affect the strength of repulsive interactions in the corona. The rest of the paper is organized as follows: in section Model and General Considerations we specify our model of the $(AB)_p$ star block copolymer. In section Polyelectrolyte Coronal Domain we calculate the pulling force exerted by the corona A-blocks onto the core blocks as a function of variable charge parameters and ionic strength of the solution. In section Core Domain we consider the B-core domain and analyze conformation of a collapsed in poor solvent star homopolymer subjected to radial extensional deformation. Our main results in terms of the phase diagrams and analysis of the character of the intramolecular unfolding transition in the $(AB)_p$ star block copolymer are presented in section Conformational Transition in $(AB)_p$ Star Block Copolymer. The analytical results are compared to the detailed self-consistent field (SCF) modeling in section SCF Modeling. In the end, we summarize our conclusions and present an outlook for the future work.

MODEL AND GENERAL CONSIDERATIONS

We consider a dilute aqueous solution of $(AB)_p$ star copolymers. A star comprises p AB diblock copolymer arms, each consisting of a hydrophobic block B with the degree of polymerization N_B and a polyelectrolyte block A with the degree of polymerization N_A. The arms are grafted by the ends of the B-blocks to a small sphere with the radius r_0. Both blocks are assumed to be intrinsically flexible. That is, the statistical segment length is of the order of a monomer unit length a. The block A comprises a fraction α_b of permanently charged monomer units, i.e., is a quenched polyelectrolyte. Water is assumed to be a marginal good solvent for both charged and uncharged monomer units of the A-block. The short-range interactions between A monomers are modeled in terms of the virial expansion, and only the pair monomer−monomer interactions with second virial coefficients v_A are considered to be relevant. On the contrary, for the hydrophobic block B water is a poor solvent, the short-range (van der Waals) interactions between B monomers are modeled in terms of Flory−Huggins parameter χ_B, under poor solvent conditions $\chi_B > 0.5$. Below we consider only very dilute solution of $(AB)_p$ star copolymer where the interactions between the stars

are weak and do not affect their conformations. To develop an analytical theory, we use a simple model assuming that all hydrophobic B blocks are equally (but not uniformly) stretched so all the A−B junction points are located at the interface on the equal distance R from the center of the star. Then all hydrophobic B blocks are within the sphere of the radius R while the coronal A blocks form a swollen brush on the surface of this sphere. This approximation is verified and justified below by detailed assumption-free numerical SCF calculations. Equilibrium value of R corresponds to the minimum of the free energy of the star:

$$F(R) = F_A(R) + F_B(R) \quad (1)$$

where F_X are contributions of hydrophilic (X = A) and hydrophobic (X = B) blocks. Minimization of the free energy, eq 1, is equivalent to the force balance condition

$$f_A(R) + f_B(R) = 0 \quad (2)$$

where $f_X(R) = dF_X(R)/dR$ are the forces acting from the block X (X = A, B) on the phantom surface separating the blocks. In the absence of the corona hydrophobic B blocks collapse and form spherical core with the radius R_0. This core preserves its shape in the amphiphilic star if the corona pulling force $f_A(R_0)$ is not sufficiently strong. With increasing pulling force (for example, caused by a decrease in the ionic strength) it reaches a certain threshold value which is enough to surmount the core restoring force corresponding at least to partial unfolding of the hydrophobic core. Obviously, this threshold is higher for more hydrophobic core. As it will be demonstrated below, in a wide range of pulling forces, inner hydrophobic part of the $(AB)_p$ star has the shape of an "octopus" (compare with ref 19) with reduced dense spherical core and stretched B branches similar to extended hydrophilic corona branches. At very high pulling forces globular core disappears, and the B blocks acquire stretched in the radial direction conformation.

In the following two sections we consider separately the swollen polyelectrolyte corona and hydrophobic core domain and derive the dependences of the free energy as well as those of pulling and reaction forces on the radial position of the junction points. The obtained dependences will be then used for analysis of equilibrium conformation of the $(AB)_p$ star as a whole.

POLYELECTROLYTE CORONAL DOMAIN

To calculate the corona free energy, we use the approach developed by Zhulina et al.[13] Consider a polymer brush composed by p chains uniformly grafted onto impenetrable sphere with the radius R. The free energy of the brush (per chain) can be expressed as

$$\frac{F}{k_B T} = \frac{3}{2a^2}\int_R^D \left(\frac{dr}{dn}\right) dr + \int_R^D f_{int}\{c_p(r)\}s(r)\, dr \quad (3)$$

where f_{int} is the free energy density of interactions in k_BT units. The latter equation implies that the end segments of all the A blocks are located at distance D from the center of the star; i.e. equal (but nonuniform!) stretching of the A blocks is preassumed. The first term describes elastic stretching of the chain. The local chain extension dr/dn is related to the local polymer concentration $c_p(r)$

$$c_p(r) = \frac{dn}{s(r)\, dr} = \frac{dn}{dr}\frac{p}{4\pi r^2} \quad (4)$$

$s(r)$ is the area per chain at the distance r from the center of the grafting sphere:

$$s(r) = \frac{4\pi}{p} r^2 \quad (5)$$

The second term in eq 3 describes excluded volume and electrostatic interactions within the star and can be represented as

$$f_{int}\{c_p(r)\} = f_{ev}\{c_p(r)\} + f_{ion}\{c_p(r)\} \quad (6)$$

where

$$f_{ev}\{c_p(r)\} = v_A {c_p}^2(r) \quad (7)$$

accounts for the excluded volume interactions in the corona. To specify the electrostatic contribution $f_{ion}\{c_p(r)\}$ for ionic corona, the combination of the mean-field and the local electroneutrality approximation (LEA) is used. The LEA assumes that the local charge of polyelectrolyte coronal chains is compensated by the excess local concentration of counterions (including oppositely charged "own" polyelectrolyte counterions and salt ions). All ions in the system are monovalent. The LEA is applicable provided that the number of block copolymer arms in one star is sufficiently large so that the excess electrostatic potential is great enough to retain the mobile counterions inside the corona, even at low salt concentrations in the solution. In the LEA framework, the electrostatic interactions manifest themselves through the translational entropy of the ions, disproportionated between the interior of the corona and the bulk solution. The concentrations (the chemical potentials) of all mobile ions in the bulk of the solution are assumed to be fixed. The distribution of mobile co- and counterions between interior of the corona and the bulk solution is determined according to the Donnan rule. The details of the approach can be found in ref 13. For strong (quenched) polyelectrolyte with constant degree of ionization α_b, it is given by[13]

$$f_{ion}\{c_p(r)\} = -\left(\sqrt{1 + (\alpha_b c_p(r)/\Phi_{ion})^2} - 1\right)\Phi_{ion} - \alpha_b c_p(r)\ln\left(\sqrt{1 + (\alpha_b c_p(r)/\Phi_{ion})^2} - \alpha_b c_p(r)/\Phi_{ion}\right) \quad (8)$$

where $\Phi_{ion} = \Sigma_j c_{bj}$ is the bulk concentration of all monovalent ions species. Therefore, the free energy can be expressed as

$$\frac{F}{k_B T} = \int_R^D f\{c_p(r), r\}s(r)\, dr \quad (9)$$

where

$$f\{c_p(r), r\} = \frac{3}{2a^2}\left(\frac{p}{4\pi}\right)^2 \frac{1}{r^4 c_p(r)} + f_{int}\{c_p(r)\} \quad (10)$$

is the free energy density. The outermost radius of the corona D is related to the polymer concentration profile $c_p(r)$ via the constraint of conservation of the total number of monomers

$$\int_R^D c_p(r)s(r)\, dr = \frac{4\pi}{p}\int_R^D c_p(r)r^2\, dr = N_A \quad (11)$$

In the following we employ the so-called local or quasi-planar (QP) approximation[13] where instead of minimization of the functional, eq 9, with respect to $c_p(r)$ the local condition of

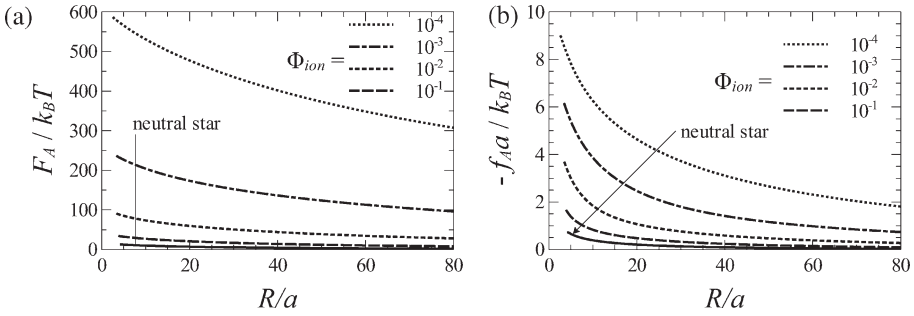

Figure 2. Free energy of polyelectrolyte corona (per chain) (a) and corresponding pulling force (b) as functions of the core radius for different salt concentrations, $\phi_{ion} \equiv \Phi_{ion}a^3$. The values of parameters are $N_A = 1000$, $p = 20$, $\alpha_b = 0.5$, and $\nu_A = a^3/6$.

vanishing the differential osmotic pressure in the corona:

$$\pi(r) = c_p^2(r)\frac{\delta}{\delta c_p(r)}\left(\frac{f\{c_p(r), r\}}{c_p(r)}\right) = 0 \tag{12}$$

is used. This leads to the following equation for $c_p(r)$:

$$-\frac{3}{a^2}\left(\frac{p}{4\pi}\right)^2\frac{1}{r^4 c_p^3(r)} + \nu_A + \Phi_{ion}\frac{\sqrt{1 + (\alpha_b c_p(r)/\Phi_{ion})^2} - 1}{c_p^2(r)} = 0 \tag{13}$$

from what the polymer density profile follows. Explicitly, it can be found only in the "inverse form" $r = r(c_p)$

$$r = \left(\frac{p}{4\pi}\right)^{1/2}\frac{3^{1/4}}{a^{1/2}c_p^{1/4}[\nu_A c_p^2 + \Phi_{ion}(\sqrt{1 + (\alpha_b c_p/\Phi_{ion})^2} - 1)]^{1/4}} \tag{14}$$

Then, the normalization condition, eq 11, can be rewritten as an integral over c_p:

$$\frac{4\pi}{p}\int_R^D c_p(r)r^2\,dr = \frac{4\pi}{p}\int_{c_p(R)}^{c_p(D)} c_p r^2(c_p)\frac{dr(c_p)}{dc_p}dc_p = N_A \tag{15}$$

The free energy functional can be written as

$$\frac{F_A}{k_BT} = \frac{4\pi}{p}\int_R^D f\{c_p(r), r\}r^2\,dr = \frac{4\pi}{p}\int_{c_p(R)}^{c_p(D)} f(c_p)r^2(c_p)\frac{dr(c_p)}{dc_p}dc_p \tag{16}$$

where $f(c_p)$ is obtained from $f\{c_p(r),r\}$, eq 10, by using eq 14

$$f(c_p) = \frac{3}{2}\nu_A c_p - \frac{1}{2}\Phi_{ion}[\sqrt{1 + (\alpha_b c_p/\Phi_{ion})^2} - 1)] - \alpha_b c_p \ln[\sqrt{1 + (\alpha_b c_p/\Phi_{ion})^2} - \alpha_b c_p/\Phi_{ion})] \tag{17}$$

We can obtain the dependence of the free energy F_A as a function of the core radius R as follows. Polymer concentration at the core surface, $c_p(R)$, is related to the core radius R via eq 13 or 14. Once parametrically $c_p(R)$ is known, the polymer concentration at the periphery of the brush, $c_p(D)$, is found using normalization condition, eq 15; then, finally we use eqs 16 and 17 to find F_A. The stretching (pulling) force from the corona side applied to the B blocks at the A−B junction points is expressed as

$$f_A = \frac{dF_A}{dR} = k_BT\frac{4\pi}{p}\left[f\{c_p(D)\}D^2\frac{\partial D}{\partial R} - f\{c_p(R)\}R^2\right] = -k_BT\frac{4\pi}{p}R^2 f\{c_p(R)\}\left[1 - \frac{f\{c_p(D)\}}{f\{c_p(R)\}}\frac{c_p(R)}{c_p(D)}\right] \tag{18}$$

$\partial D/\partial R$ is found by differentiating the normalization condition eq 11 with respect to R. Figure 2 shows the free energy and pulling force dependences of the radius R calculated for $N_A = 1000$, $p = 20$, $\alpha_b = 0.5$, $\nu_A = a^3/6$, and various volume fractions of salt, $\phi_{ion} \equiv \Phi_{ion}a^3$. Both F_A and f_A are decreasing functions of R; a decrease in the ionic strength leads to an increase of the pulling force f_A.

CORE DOMAIN

The core domain of the $(AB)_p$ star can be considered as a polymer star under poor solvent conditions with each arm subjected to radial tension exerted by the swollen coronal blocks. The analysis of the conformations of the core blocks necessitates taking into account the specific effects appearing upon extensional deformation of a polymer globule. The latter reveals, in its turn, a nontrivial physical picture.

Extensional Deformation of a Single Chain in Poor Solvent. As it was first shown by Halperin and Zhulina,[20,21] when a constant force is applied to the ends of a polymer chain collapsed in poor solvent, there exists a critical force, below which the globule remains compact but changes its shape from spherical to prolate ellipsoidal, whereas above the critical force it unwinds into a stretched chain. When the globule is deformed in the extension ensemble, i.e., the distance between chain ends is imposed, the unfolding scenario is more complex: it occurs via formation of the "tadpole" conformation in which the spherical globular "head" coexists with the stretched string of thermal blobs ("leg"). In our recent works[22,23] we have performed a detailed self-consistent field (SCF) calculation and developed a quantitative analytical theory of the equilibrium unfolding of a globule formed by a flexible homopolymer chain collapsed in a poor solvent and subjected to an extensional deformation. Both the SCF calculations and the analytical theory prove that upon an increase in the end-to-end distance three regimes of deformation

dx.doi.org/10.1021/ma201652k |Macromolecules 2011, 44, 8999–9012

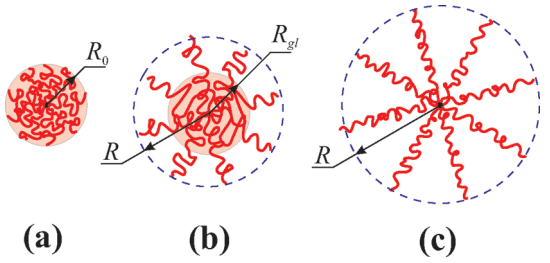

Figure 3. Polymer star collapsed in poor solvent: (a) free (unperturbed) star, (b) radially stretched star at moderate deformation, (c) strongly radially stretched star.

successively occur: at small deformation the globule acquires a prolate shape, the reaction force grows linearly with the deformation; at moderate deformations the globule is in the tadpole conformation, the tail of the tadpole is uniformly stretched, its extension as well as the reaction force is weakly decreasing with the deformation; then at certain extension the globular head unravels and the globule completely unfolds, the reaction force drops down and then grows again upon further extension (this jumpwise "unraveling transition" was first predicted by Cooke and Williams[24]). In the framework of the developed theory it was possible to calculate prolate globule−tadpole and tadpole−open chain transition points and to find corresponding conformational characteristics, such as the asymmetry and the number of monomers in the globular head, reaction forces, and force jump at transition, in a wide range of polymerization degree N and solvent quality (χ). Our analysis has shown that the system exhibits a critical point; i.e., there exists a minimal chain length $N_{cr}(\chi)$ below which, at $N < N_{cr}(\chi)$, the intramolecular microphase segregation in the extended globule does not occur. The globule is deformed as a whole, without intramolecular segregation but by progressive depletion of its core.

Homopolymer Star in Poor Solvent. Consider a free polymer star comprising p arms each of N_B monomer units immersed into a poor solvent, $\chi \geq 0.5$. The star can be represented as a spherical polymer brush grafted onto a small sphere with the radius r_0. The mean grafting area per chain is then $s_0 = 4\pi r_0^2/p$. Since p arms cover the surface of the sphere and the arm cross-section area equals to a^2, r_0 can be estimated as $r_0 = a(p/(4\pi))^{1/2}$. It is assumed that all the chains are extended equally but nonuniformly in the radial direction so that their free ends are localized at the edge of the star at the distance R_0 from its center. It can be shown[16] that the concentration profile of the collapsed star consists of three concentric regions: Close to the center, there is a narrow zone where polymer volume fraction is approximately equal to unity. Then it decays as $1/r$ down to the concentration φ, which is the characteristic globular concentration. In the Flory−Huggins model, the polymer concentration φ or, equivalently, the volume fraction in the globule $\phi \equiv \varphi a^3$ can be expressed via Flory parameter χ as[23] $\chi \simeq (\ln(1-\phi))/\phi^2 - 1/\phi$. Since the radius of the central zone of decaying concentration is small compared to the radius of the globule R_0, in the following calculation we assume that the polymer concentration in the collapsed star is uniform and equal to φ, i.e.

$$R_0 \simeq \left(r_0^3 + \frac{3N_B p}{4\pi\varphi}\right)^{1/3} \tag{19}$$

This simplification should not affect, neither qualitatively nor quantitatively, the final result. Consider now the situation where the ends of star arms are "pinned" at the distance $R \geq R_0$; i.e., each arm of the collapsed star is radially stretched. In accordance with the general picture of polymer globule deformation,[20,22] we propose the following model: we assume that under such extensional deformation the star segregates into corona formed by equally stretched "tails" and spherical globular core (Figure 3b). The polymer concentration in the core is still equal to φ whereas the tails are the uniformly stretched parts of the polymer chains exposed to the solvent. If the core contains N_{gl} monomer units per arm and has, therefore, the radius

$$R_{gl} = \left(r_0^3 + \frac{3N_{gl}p}{4\pi\varphi}\right)^{1/3} \tag{20}$$

then the free energy of the deformed star *per star arm* can be represented as follows

$$\frac{F_B}{k_B T} = \frac{3}{2a^2}\int_{r_0}^{R_{gl}}\left(\frac{dr}{dn}\right)dr + \mu N_{gl} + \gamma\frac{4\pi R_{gl}^2}{p} + \frac{3(R-R_{gl})^2}{2(N_B - N_{gl})a^2} \tag{21}$$

where the first term is the elastic free energy of the globular core (r is the radial coordinate and n is the monomer ranking number counted within each arm from the center of the star), $k_B T\mu$ is the monomer chemical potential (free energy) in the infinite globule (μ is negative under poor solvent conditions), the third term accounts for the interfacial contribution from the surface of the globule, $k_B T\gamma$ is the interfacial tension coefficient (γ is positive due to the energetic and conformational penalty of redundant monomer−solvent contacts at the interface), and the last term is the elastic free energy of the tail. In the volume approximation, which is applicable for sufficiently large core, it is assumed that both μ and γ are functions of the solvent quality only (i.e., independent of the core size); their dependences on the Flory parameter χ are expressed as follows: the monomer chemical potential μ can be found, once the polymer volume fraction within the globule, ϕ, is known:[23]

$$\mu = 2 + \frac{2-\phi}{\phi}\log(1-\phi) \tag{22}$$

For the interfacial tension coefficient $k_B T\gamma$ an explicit expression can be obtained for moderately poor solvent only:[23,25]

$$\gamma a^2 = \frac{3}{16}(1-2\chi)^2 \tag{23}$$

Comparison with the values of γ obtained numerically using Scheutjens−Freer self-consistent field (SF-SCF) approach shown[23] that this approximation works good for $\chi \lesssim 1.2$, which is the range of χ we are interested in. Since the polymer concentration in the globule is constant and equal to φ, local chain tension is $dr/dn = p/(4\pi r^2\varphi)$, and the integral in eq 21 can be easily calculated

$$\frac{F_B}{k_B T} = \frac{3p}{8\pi a^2\varphi}\left(\frac{1}{r_0} - \frac{1}{R_{gl}}\right) + \mu N_{gl} + \gamma\frac{4\pi R_{gl}^2}{p} + \frac{3(R-R_{gl})^2}{2(N_B - N_{gl})a^2} \tag{24}$$

dx.doi.org/10.1021/ma201652k |*Macromolecules* 2011, 44, 8999–9012

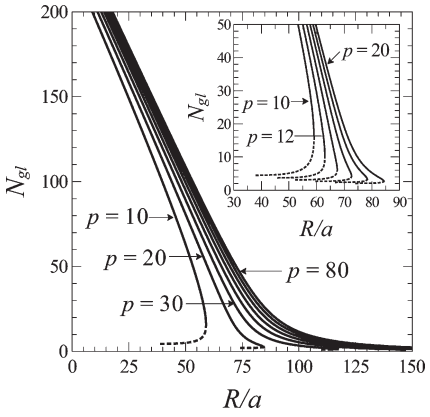

Figure 4. Number of monomers in the star core N_{gl} as a function of the star deformation R calculated using eq 27 for $\chi = 1$, $N_B = 200$, and various values of $p = 10, 20, 30, ..., 80$ in the main figure and $p = 10, 12, 14, ..., 20$ in the inset. Dashed parts of the curves correspond to unphysical solution.

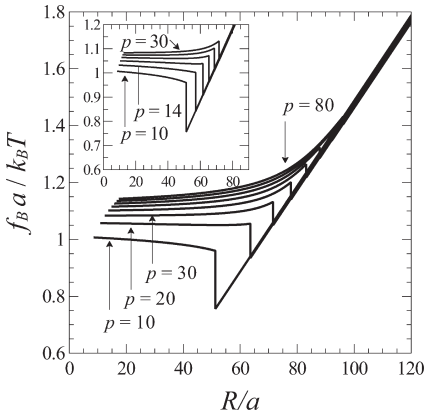

Figure 5. Equilibrium force−extension curves for $\chi = 1$, $N_B = 200$, and various values of $p = 10, 20, 30, ..., 80$ in the main Figure and $p = 10, 14, 18, ..., 30$ in the inset.

To find the equilibrium value of N_{gl} at given R, the free energy, eq 24, should be minimized with respect to N_{gl}:

$$\frac{dF_B}{dN_{gl}} = \frac{\partial F_B}{\partial N_{gl}} + \frac{\partial F_B}{\partial R_{gl}}\frac{\partial R_{gl}}{\partial N_{gl}} = 0 \tag{25}$$

which leads to the following equation:

$$\frac{3p^2}{32\pi^2\varphi^2 {R_{gl}}^4 a^2} + \gamma\frac{2}{\varphi R_{gl}} - \frac{3p(R - R_{gl})}{4\pi\varphi {R_{gl}}^2 (N_B - N_{gl})a^2} + \mu + \frac{3(R - R_{gl})^2}{2(N_B - N_{gl})^2 a^2} = 0 \tag{26}$$

Solution of eq 26 should give the equilibrium number of monomer units (in a star arm), N_{gl}^{eq}, that remain in the globular core as a function of the imposed star deformation R. Equation 26 can be resolved analytically with respect to $R = R(N_{gl})$. The solution is as follows:

$$R = R_{gl} + (N_B - N_{gl})a\left[\frac{p}{4\pi\varphi {R_{gl}}^2 a} + \sqrt{-\frac{2}{3}\mu - \frac{4\gamma}{3\varphi R_{gl}}}\right] \tag{27}$$

where $R_{gl} = R_{gl}(N_{gl})$ is given by eq 20. Let us consider eqs 27 and 20 as an implicit dependence of the number of monomer units in the core, N_{gl}, on the given value of the star extension R. Figure 4 shows a family of N_{gl} vs R curves for $N_B = 200$, $\chi = 1$, and various number of arms p. Solid lines show solutions corresponding to N_{gl} that decreases with increasing extension R whereas dashed lines show unphysical situation (simultaneous increase of the deformation R and of the amount of the polymer condensed in the globular core) and should be therefore excluded from our consideration. The point where $dR/dN_{gl} = 0$ represents a spinodal point where the two-phase "octopus" state (Figure 3 b) loses its stability. It corresponds to the (i) largest possible extension and (ii) smallest possible core size for the locally stable microsegregated deformed star. It can bee seen that for moderate values of p the smallest number of monomer units in the core $N_{gl,min} > 1$; for instance, at $p = 20$, $N_{gl,min} \approx 2.7$. As p grows $N_{gl,min}$ decreases and assumes values less than unity.

By substituting eq 27 into eq 24, one obtains the equilibrium free energy of the segregated deformed star (Figure 3b) as a function of N_{gl}; the latter expression together with eq 27 provides a parametric dependence of $F_B(R)$. This free energy should be compared with that of completely unfolded star which has no globular core (Figure 3c)

$$\frac{F_B^{(unfolded)}}{k_B T} = \frac{3(R - r_0)^2}{2N_B a^2} \tag{28}$$

to decide which state of the star (partly or completely unfolded) is thermodynamically stable. The comparison of the free energies of the star with partially and completely unfolded arms enables us to localize the first-order transition point between these two conformations and to calculate the magnitude of the jump-down in the reaction force. As follows from results presented in Figure 5, an increase in the number of arms leads to the shift of the transition point toward larger values of deformation R and to a decrease in the magnitude of the force jump. The reaction force f_B per arm of the partially unfolded core is

$$f_B(R) = \frac{dF_B}{dR} = \frac{\partial F_B}{\partial R} + \frac{\partial F_B}{\partial N_{gl}}\frac{\partial N_{gl}}{\partial R} = \frac{3(R - R_{gl})}{(N_B - N_{gl})a^2} k_B T \tag{29}$$

Using eq 27, we can express f_B as a function of R_{gl}:

$$\frac{f_B(R_{gl})}{k_B T} = \frac{3}{a}\left[\frac{p}{4\pi\varphi {R_{gl}}^2 a} + \sqrt{-\frac{2}{3}\mu - \frac{4\gamma}{3\varphi R_{gl}}}\right] \tag{30}$$

The reaction force per arm of completely unfolded/unraveled star is

$$f_B^{(unfolded)}(R) = \frac{\partial F_B^{(unfolded)}}{\partial R} = \frac{3(R - r_0)}{N_B a^2} k_B T \tag{31}$$

Figure 5 shows equilibrium force−extension curves calculated for the set of parameters ($N_B = 200$, $\chi = 1$) similar to that in Figure 4. It can be seen that if the number of star arms is small ($p = 10$ or 14 in Figure 5), the force−extension curve looks very similar to that for a single chain.[22,23] There is, however, a tiny difference in the initial part of the force−deformation curves: For the star the curve starts at $R = R_0$ with a nonzero force. This is because in the present work we do not consider an initial deformation regime that could lead to a distortion of the spherical

symmetry of the collapsed star or to a decrease in the mean polymer concentration φ within the star. Hence, a pulling force which is less than the threshold force that gives rise to the microphase segregation does not affect the structure of collapsed star. The value of this threshold force can be easily obtained from eq 30 by setting $N_{gl} = N_B$ and $R_{gl} = R_0$:

$$\frac{f_{B,\min}}{k_B T} = \frac{3}{a}\left[\frac{p}{4\pi\varphi {R_0}^2 a} + \sqrt{-\frac{2}{3}\mu - \frac{4\gamma}{3\varphi R_0}}\right] \quad (32)$$

One can see that the threshold force grows with increasing number of arms in the star p. A similar effect is observed for a globule formed by a linear macromolecule: the value of the force corresponding the onset of the microphase segregation in the deformed globule grows as the degree of polymerization increases. In the star case the overall molecular weight is $N_B p$, and this causes the effect. In the phase segregation regime, the force for the star with $p = 10$ weakly decreases as a function of the arm extension; in the "unraveling" transition point it drops down and then grows as $3(R - r_0)/(N_B a^2) \simeq 3R/(N_B a^2)$ for the unfolded star. However, with an increase in p the character of the force−extension curves changes: the slope of the quasi-plateau on the $f_B(R)$ curve becomes less negative and can even be positive. To estimate the slope of the force−extension curve, the derivative df_B/dR should be calculated. Since the reaction force is given in eq 30 as a function of R_{gl}, it is expressed as follows:

$$\frac{df_B}{dR} = \frac{\partial f_B}{\partial R_{gl}}\frac{\partial R_{gl}}{\partial N_{gl}}\frac{dN_{gl}}{dR} \quad (33)$$

Since $\partial R_{gl}/\partial N_{gl} > 0$ and $dN_{gl}/dR < 0$, the sign of df_B/dR is opposite to that of $\partial f_B/\partial R_{gl}$. The expression for $\partial f_B/\partial R_{gl}$ can easily be found:

$$\frac{\partial}{\partial R_{gl}}\left(\frac{f_B}{k_B T}\right) = \frac{3}{a}\left[-\frac{p}{2\pi\varphi {R_{gl}}^3 a} + \frac{2\gamma}{3\varphi {R_{gl}}^2\sqrt{-\frac{2}{3}\mu - \frac{4\gamma}{3\varphi R_{gl}}}}\right] \quad (34)$$

We see that at small p the second positive term in square brackets in eq 34 related to the globule's surface tension dominates, then $df_B/dR < 0$, and the quasi-plateau has a negative slope, whereas for large p the first negative term dominates and this corresponds to the increasing quasi-plateau. The threshold value of $p = p^*$ at which the negative-to-positive change in the quasi-plateau slope occurs can be easily found by considering the initial part of the force−extension curve where $N_{gl} = N_B$, $R_{gl} = R_0$. If $p = p^*$ corresponds to $\partial f_B/\partial R_{gl} = 0$, this leads to the following equation:

$$-\frac{p}{2\pi\varphi R_0 a} + \frac{2\gamma}{3\varphi\sqrt{-\frac{2}{3}\mu - \frac{4\gamma}{3\varphi R_0}}} = 0 \quad (35)$$

We can find an explicit solution of the latter equation if we take $R_0 \simeq (3N_B p/4\pi\varphi)^{1/3}$ and $[-(2/3)\mu - (4\gamma)/(3\varphi R_0)]^{1/2} \simeq (-(2/3)\mu)^{1/2}$. With these simplifications we obtain

$$p^* = 4\pi\left(\frac{3N_B}{\varphi a^3}\right)^{1/2}\frac{(\gamma a^2)^{3/2}}{(-6\mu)^{3/4}} \quad (36)$$

Hence, p^* increases upon an increase in solvent strength for the B block. For the case $N_B = 200$, $\chi = 1$ presented in Figures 4 and 5, eq 36 gives $p^* \approx 25$, which is in accordance with the results presented in the inset in Figure 5. Note also that according to eq 36 p^* scales as a square root of arm length N_B. At the same time, as p increases, the drop in the reaction force that accompanies the unraveling transition decreases. This is in accordance with the conclusion made for a deformed single globule where the force jump at the tadpole−uniformly stretched chain transition decreases as the overall chain length N increases.

■ CONFORMATIONAL TRANSITION IN $(AB)_p$ STAR BLOCK COPOLYMER

In the preceding sections, the expressions for the core and the corona free energies and corresponding forces were obtained. Consider now the $(AB)_p$ core−shell star as a whole. Figure 6 presents as an example the free energy of the star $F(R) = F_A(R) + F_B(R)$ as a function of the radial position R of the A−B junction points at different salt concentrations. ($F_A(R)$ and $F_B(R)$ were calculated using expressions obtained in the previous sections.) An equilibrium conformation of the star corresponds to a (global) free energy minimum. The latter is equivalent to the core and corona force balance condition, eq 2; i.e., alternatively we can consider force f vs radius R dependences. Such dependences corresponding to the case presented in Figure 6 are shown in Figure 7: for the core, there is a single curve starting at $r = R_0$, while for the corona, there is a family of curves that corresponds to different salt concentrations. Figure 7 can also be considered as a (partial) superposition of Figures 2b and 5.

At relatively high salt concentration, $\phi_{ion} = 10^{-1}$, the electrostatic repulsions are weak, and as a result, the pulling force from the corona with the inner radius R_0, eq 19, is smaller than the threshold force, eq 32, necessary for unfolding of the core. We see that in this regime the free energy has one boundary minimum corresponding to a unimolecular micelle with collapsed core ($R = R_0 = (3Np/4\pi\varphi)^{1/3}$). Correspondingly, the $|f_A(R)|$ curve does not cross $f_B(R)$ dependence, as it can be seen in Figure 7.

At lower salt concentration $\phi_{ion} = 10^{-2}$, which is below certain salt concentration threshold, $|f_A(R)|$ curve crosses the $f_B(R)$ curve in the microphase segregation ("octopus") regime at $R > R_0$. This point corresponds to the local (nonboundary) minimum of the free energy $F(R)$. A similar picture is observed at $\phi_{ion} = 10^{-3}$; the equilibrium radius of the B-domain, R, is shifted toward larger values. At $\phi_{ion} = 10^{-4}$ the free energy minimum and the point of intersection of $|f_A(R)|$ and $f_B(R)$ curves correspond to the conformation with completely unfolded core. Remarkably, close to the transition point between the conformations with partially and fully unfolded core, the free energy has two minima. (This can be seen on curves for $\phi_{ion} = 10^{-3}$ in Figure 6; in Figure 7 two points of intersection are clearly seen.) Besides the main minimum corresponding to the octopus-like conformation, the second metastable minimum related to completely unfolded core appears. The appearance of the two minima in the free energy implies coexistence of the stars with the partially and completely unfolded core domain and signifies quasi-first-order character of the unfolding transition: Upon a decrease in ϕ_{ion} the system "jumps" from the "left-hand-side" minimum (corresponding to the microphase-segregated partially unfolded core) to the "right-hand-side" minimum (corresponding to the star with completely unfolded core domain). For the set of parameters used here, the coexistence between microphasely

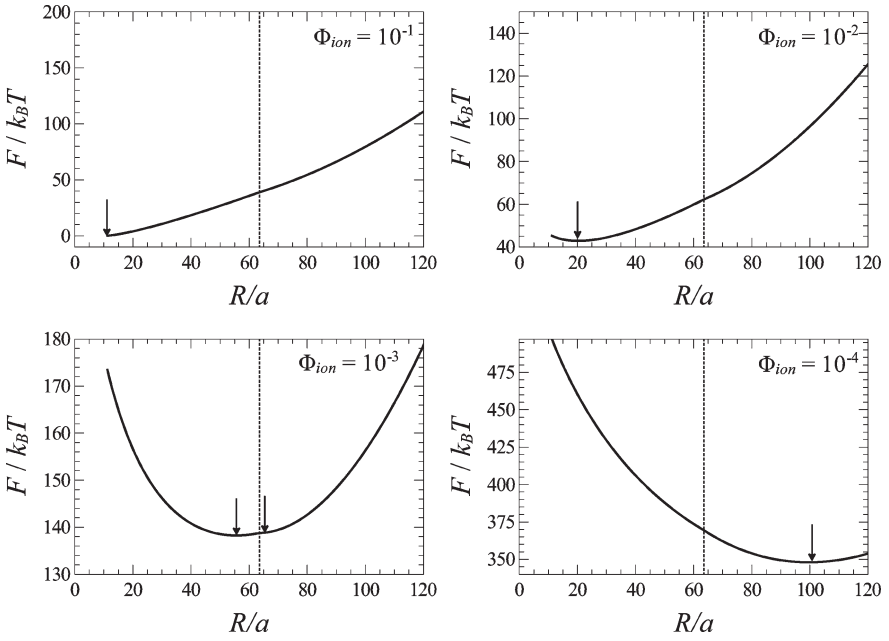

Figure 6. Free energy of $(AB)_p$ core−shell star with $p = 20$, $N_A = 1000$, $N_B = 200$, $v_A = a^3/6$, $\chi_B = 1$, $\alpha_b = 0.5$, and different values of ϕ_{ion}. Arrows show the position of local or boundary minima, and dashed line separates regions of partially and completely unfolded core.

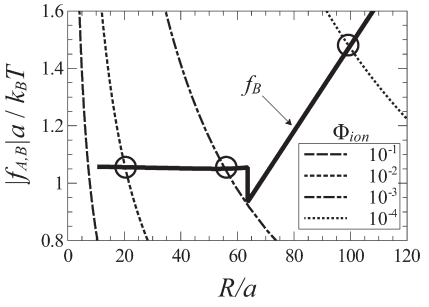

Figure 7. Core reaction force (gray curve) and corona pulling force (black curves) in $(AB)_p$ core−shell star with $p = 20$, $N_A = 1000$, $N_B = 200$, $v_A = a^3/6$, $\chi_B = 1$, $\alpha_b = 0.5$, and different values of ϕ_{ion}. Circles show the position of equilibrium between the core and the corona.

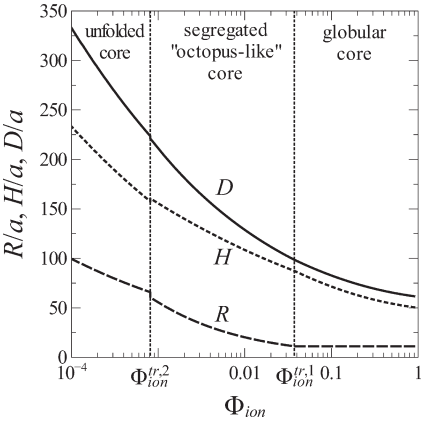

Figure 8. Core radius R (dashed line), corona thickness H (dotted line), and overall star radius $D = R + H$ (solid line) as functions of ionic strength. Parameters of the $(AB)_p$ star: $p = 20$, $N_A = 1000$, $N_B = 200$, $v_A = a^3/6$, $\chi_B = 1$, and $\alpha_b = 0.5$. Vertical dotted lines separate different star regimes.

segregated and fully unfolded core occurs at $R \approx 61$, as it is shown in by a vertical dashed line in Figure 6. Figure 8 shows equilibrium position R of the A−B junction points, the overall star radius D (which is, equivalently, the outermost corona radius), and the corona thickness $H = D - R$ as functions of salt concentration ϕ_{ion}. As we have shown, with a decrease in ϕ_{ion} the star undergoes a sequence of intramolecular conformational transitions: when salt concentration is large, repulsive interactions in the corona are weak and the core keeps the spherical collapsed shape with the radius R_0. The corona thickness and overall star size increase in this regime upon a decrease in salt concentration due to progressively increasing differential osmotic pressure inside the corona. Simultaneously, the pulling force applied to the ends of the B-blocks localized at the surface of the core domain increases. At certain threshold salt concentration $f_A(R_0)$ becomes equal to the critical minimum force $f_{B,min}$ given by eq 32. This point corresponds to the onset of the microphase segregation within the core and appearance of the stretched "legs". From this point on, a decrease in salt concentration leads to a progressive unfolding of the core, an increase in the length of the "legs", and, consequently, an increase in R, D, and H, which is interrupted by abrupt transition from partially to completely unfolded core conformation. In the transition point the core size R increases jumpwise, and this causes a simultaneous jumpwise decrease of the corona thickness H. This drop in the corona thickness occurs because of increasing distance between the A−B junction points and decreasing crowding of the A-blocks in the coronal domain. However, as a result of these two opposite tendencies, the overall (outermost) size of the star D exhibits a small jump up. In the low salt regime where the core is completely unfolded, R, D, and H grow again progressively as ϕ_{ion} decreases.

We see that a progressive decrease in ϕ_{ion} causes, in a sequence, two intermolecular conformational transitions: The first one

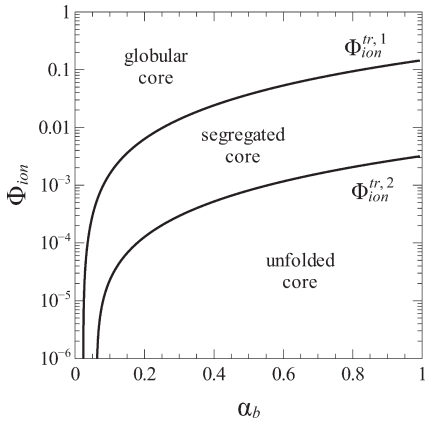

Figure 9. Diagram of states of amphiphilic $(AB)_p$ core−shell star with $p = 20$, $N_A = 1000$, $N_B = 200$, $v_A = a^3/6$, and $\chi_B = 1$ on the $(\alpha_b;\phi_{ion})$ plane. $\phi_{ion}^{tr,1}$ and $\phi_{ion}^{tr,2}$ are the ionic strengths corresponding to the onset of microphase segregation in the core and to complete core unfolding, respectively.

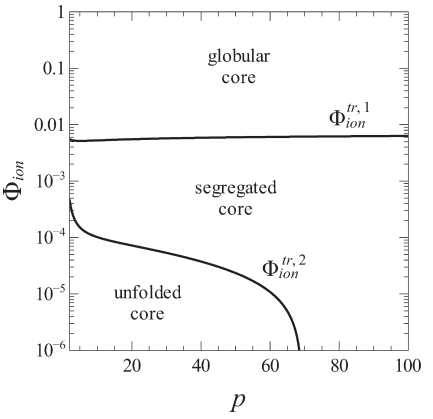

Figure 10. Diagram of states of amphiphilic $(AB)_p$ core−shell star with $N_A = 500$, $N_B = 200$, $v_A = 1/6$, $\chi_B = 1$, and $\alpha_b = 0.2$ on the $(p;\phi_{ion})$ plane. $\phi_{ion}^{tr,1}$ and $\phi_{ion}^{tr,2}$ are the ionic strengths corresponding to the onset of microphase segregation in the core and to complete core unfolding, respectively.

corresponds to the continuous onset of the microphase segregation within the core, whereas the second one is the jumpwise transition corresponding to the complete unfolding of the core (vanishing of the globular phase). We denote the salt concentrations at which these transitions occur as $\phi_{ion}^{tr,1}$ and $\phi_{ion}^{tr,2}$, respectively. Their values are determined by the parameters of the $(AB)_p$ core−shell star (N_A, N_B, p, α_b, v_A, χ_B); therefore, a multidimensional diagram of states can be constructed. Figures 9 and 10 represent two-dimensional sections of the such a diagram of states in coordinates (α_b,ϕ_{ion}) and (p,ϕ_{ion}), respectively. As follows from the analysis of the first diagram, Figure 9, if the fraction of charged monomers α_b in the corona block A is small (below a certain threshold value $\alpha_{b,min}$), the electrostatic interactions in the corona are not strong enough to induce the unfolding of the collapsed core even at vanishing ionic strength of the solution. The value of $\alpha_{b,min}$ is controlled by the hydrophobicity of the core forming blocks and can be expressed as

$$\alpha_{b,\,min} \sim \left(\frac{af_{B,\,min}}{k_B T}\right)^2 \tag{37}$$

where $f_{B,min}$ is given by eq 32. Moreover, if α_b is only slightly larger than $\alpha_{b,min}$, a decrease in the ionic strength stabilizes the microphase-segregated state of the core, whereas the complete core unfolding does not occur even in the salt-free solution.

The diagram of states in (ϕ_{ion},p) coordinates (Figure 10) allows us to analyze the influence of the number of the star arms p on the character of the conformational transitions related to the core unfolding. The diagram presented in Figure 10 shows that $\phi_{ion}^{tr,1}$ corresponding to the onset of the microphase segregation in the core is only a weakly increasing function of p. By contrast, the characteristic salt concentration $\phi_{ion}^{tr,2}$ corresponding to the jumpwise complete core unfolding is a decreasing function of p which approaches zero at some finite value of p ($p \approx 70$ for our set of parameters). In the stars with larger number of arms the core unfolding occurs continuously upon a decrease in the salt concentration. This behavior is related to a decrease of number of monomers in the "minimal core" and a decrease in the magnitude of the jump in the A−B junction points position upon transition from the microphase-segregated to completely unfolded state as p increases (see Figure 5 and section Core Domain). Hence, the microphase-segregated region on the phase diagram in Figure 10 extends at large p to low salt concentration, but one should realize that at small ϕ_{ion} the core is (almost) completely unfolded.

SCF MODELING

To check the validity of our theoretical predictions and the correctness of the underlying model assumptions, we use Scheutjens−Fleer self-consistent field (SF-SCF) numerical approach to study the structure of the AB core−shell star and conformational rearrangements upon changes in environmental conditions, i.e., upon change in the ionic strength.

SCF Formalism. The self-consistent field (SCF) method is well-known for the modeling of inhomogeneous polymer layers. At the basis of the approach is a mean-field free energy which is expressed as a functional of the volume fraction profiles (normalized concentrations) and self-consistent field potentials. The optimization of this free energy leads for Gaussian polymer chains to the Edwards diffusion (ED) differential equation,[26] which for an arbitrary coordinate system may be expressed as

$$\frac{\partial G(\mathbf{r},\mathbf{r}';n)}{\partial n} = \frac{a^2}{6}\nabla^2 G(\mathbf{r},\mathbf{r}';n) - \frac{u(\mathbf{r})}{k_B T}G(\mathbf{r},\mathbf{r}';n) \tag{38}$$

where k_B is the Boltzmann constant, T is the absolute temperature, and a is the monomer unit size. Green's function $G(\mathbf{r},\mathbf{r}';n)$ used in eq 38 is the statistical weight of a probe chain with the length n having its ends fixed in the points $\mathbf{r}'$ and $\mathbf{r}$. The self-consistent potential $u(\mathbf{r})$ represents the surrounding of the chain and serves as an external field used in the Boltzmann equation to find the statistical weight for each chain conformation. Consequently, Green's functions $G(\mathbf{r},\mathbf{r}';n)$ that obey eq 38 are related to the volume fraction profile of the polymer $\varphi(\mathbf{r})$ or, in the case of a multicomponent system, to the set of volume fraction profiles $\varphi_k(\mathbf{r})$ where $k = 1, 2, \ldots$ specifies the component. As long as the potential $u(\mathbf{r})$ is local (i.e., there are no long-range forces), it depends on the local volume fraction $\varphi(\mathbf{r})$. The electrostatic interactions in the system are taken into account on the level of the Poisson−Boltzmann approximation: local electrostatic potential is calculated from the Poisson equation, which accounts for the charge density distribution

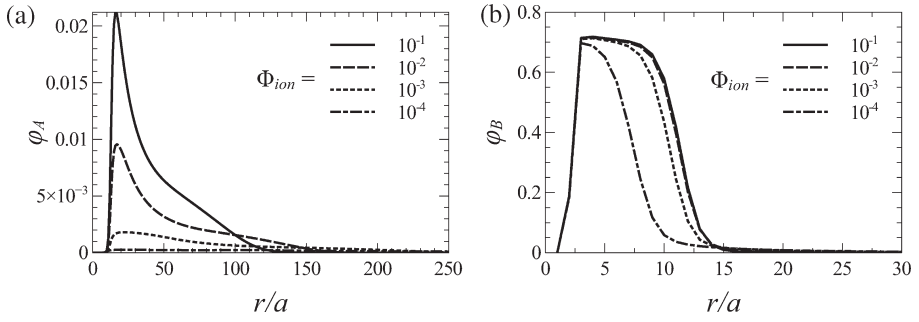

Figure 11. Radial density profiles of A monomers (a) and B monomers (b) in AB core−shell star with $p = 20$, $N_A = 1000$, $N_B = 200$, $\chi_A = 0$, $\chi_B = 1$, $\alpha_b = 0.5$, and different values of ϕ_{ion} (shown in the legend).

created by all charged species (i.e., charged monomer units and mobile ions). This makes up the system of self-consistent field equations which is solved iteratively: one assumes an initial volume fraction profile $\varphi(\mathbf{r})$, then computes the potential $u(\mathbf{r})$, the set of Green's functions using eq 38, and derives a new volume fraction profile $\varphi'(\mathbf{r})$. The procedure is then repeated until the sequence of approximations converges to a stable solution. To solve these equations rigorously, it is necessary to introduce a numerical algorithm. Such numerical scheme invariably involves space discretization (i.e., the use of a lattice). Here we follow the method of Scheutjens and Fleer (SF-SCF),[27] who used the segment size a as the cell size. A mean-field approximation is applied to a set of lattice sites. This set (often called a lattice layer) is referred to with a single coordinate $\mathbf{r}$. The way the sites are organized in layers depends on the symmetry in the system and must be preassumed. The approach allows for, e.g., volume fraction gradients between these layers. In order to consider an isolated polymer star, it is enough to use a one-gradient version of SCF algorithm in the spherical coordinate system, for which $\mathbf{r} = r$. In this case, all volume fraction profiles as well as other thermodynamic values depend only on the radial coordinate r, while the mean-field approximation is used along angular coordinates. More specifically, within our model p AB diblock copolymer chains are homogeneously pinned at the surface of a small sphere with the radius $r_0 = a\lceil (p/(4\pi))^{1/2} \rceil$, where $\lceil x \rceil$ denotes is the smallest integer not less than x (the so-called ceiling function). AB copolymer nature of the chains is taken into account via the set of Flory−Huggins parameters for monomer−solvent interactions, χ_A and χ_B, and monomer−monomer cross-interactions, χ_{AB}. The solvent is assumed to be good (athermal) for A monomers, $\chi_A = 0$, and poor for B monomers, $\chi_B = 1$. We chose $\chi_{AB} = \chi_B$, meaning that the incompatibility between A and B monomers is the same as between B monomers and solvent molecules. The block A is a positively charged polyelectrolyte; with quenched charge, the fraction of charged monomer units is equal to α_b (i.e., α_b is the fractional charge per A monomer unit). There are two types of salt ions in the system: co-ions Na^+ and counterions Cl^-. SCF calculations were performed using the SFBox program developed at Wageningen Uviversity.

Results of SCF Modeling. To make a quantitative comparison with the results of the theory, we have made SCF calculations for $(AB)_p$ copolymer star with the parameters similar to those used in the previous section (Figures 6−10), that is, we consider a star with $p = 20$ AB-diblock copolymer arms (for $p = 20$ the radius of the grafting sphere is $r_0 = 2$), $N_A = 1000$, $N_B = 200$, fraction of charged A-monomers $\alpha_b = 0.5$, and monomer−solvent interaction parameters $\chi_A = 0$ (which gives for the second virial coefficient $v_A = a^3/6$) and $\chi_B = 1$. The Flory−Huggins interaction parameters for the salt ions are taken the same as for the solvent molecules. The salt volume fraction was varied in the range $10^{-1} \le \phi_{ion} < 10^{-4}$. The SF-SCF method has obvious advantages, as compared to the analytical theory, in being assumption-free: neither strong chain stretching nor equal radial positions of the junction points and terminal monomer units are preassumed. As a result, the SF-SCF approach provides a more accurate information about density distribution in the core and in the corona of the star. On the other hand, the use of one-gradient version of the SCF approach "smears out" lateral inhomogeneity of the star with microphase-segregated or unfolded core (Figure 3).

Since one of our motivations of using the SCF modeling is to check the underlying model assumptions, let us list the latters. The analytical theory was developed under assumption that (1) all hydrophobic B blocks are equally (but possibly not uniformly) stretched so all the A−B junction points are located at equal distance R from the center of the star; (2) all hydrophilic A blocks are equally (but not uniformly) stretched so all the A end points are located on the equal distance D from the center of the star; (3) core and corona (correspondingly B and A blocks) are segregated in space—there is a sharp phantom interface separating core and coronal domains; (4) at strong repulsive interaction in the corona microphase segregation in the core occurs; (5) at strong repulsive interaction in the corona stretched "legs" of the microphase-segregates "octopus" structure are *uniformly* extended; and (6) local electroneutrality approximation for the corona is fulfilled.

Figure 11 shows evolution of radial density profiles of A and B monomers with decreasing ionic strength. The density profile of the swollen corona (A units density profile, Figure 11a) has a sharp maximum at the interface between A and B domains and then decays with increasing r. A decrease in the salt concentration ϕ_{ion} leads to progressive corona swelling: the maximum value of φ_A decreases, and the profile broadens (i.e., the overall AB star size grows, in accordance with Figure 8). The density profile of hydrophobic B monomer units is qualitatively very different from its A counterpart. Figure 11b shows that at high salt concentration ($\phi_{ion} = 0.1$, 0.01) the distribution of the B units inside the core is nearly uniform, with a narrow depletion zone in the layer adjacent to the grafting point and a sharp decay at the edge of the core. With a decrease in ϕ_{ion}, the pulling force from the coronal A blocks grows and microphase segregation in the core is clearly seen. The profile has two parts: a dense core and a sparse periphery with the density much less than that of the core. As

dx.doi.org/10.1021/ma201652k |*Macromolecules* 2011, 44, 8999–9012

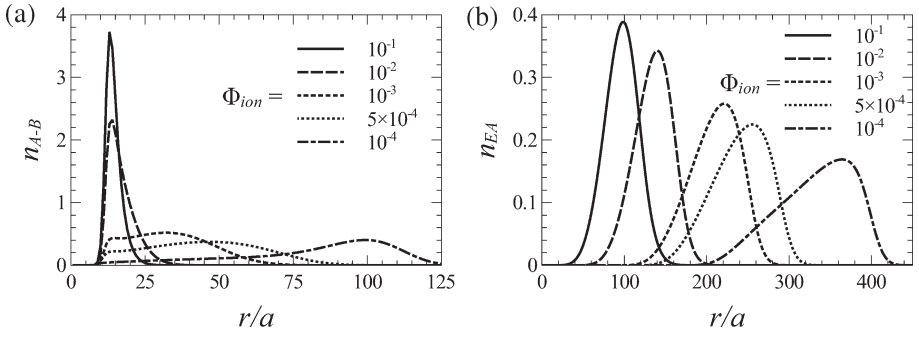

Figure 12. Radial distribution of the number of A−B junction points (a) and A end points (b) in AB core−shell star with $p = 20$, $N_A = 1000$, $N_B = 200$, $\chi_A = 0$, $\chi_B = 1$, $\alpha_b = 0.5$, and different values of ϕ_{ion}.

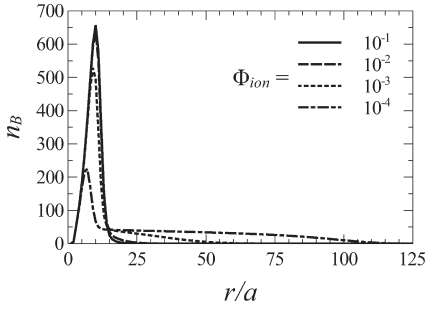

Figure 13. Radial distribution of the number of B monomer units in AB core−shell star with $p = 20$, $N_A = 1000$, $N_B = 200$, $\chi_A = 0$, $\chi_B = 1$, $\alpha_b = 0.5$, and different values of ϕ_{ion}.

ϕ_{ion} decreases, the globular core becomes smaller, and the low-density peripheral part extends at the expense of the depleted core. This picture is in accordance with our model assumption 4 about microphase segregation in the core.

Another important characteristic is the radial distribution of the number of monomers of the type i, $n_i(r)$. It is easily obtained from the corresponding radial density distribution $\varphi_i(r)$ by multiplying it by the number of lattice sites in the corresponding layer $L(r)$ (which is the volume of the spherical layer): $n_i(r) = \varphi_i(r)L(r) = \varphi_i(r)4\pi(ar^2 - a^2r + a^3/3)$. Number distribution is the best way for expressing and analyzing the distribution of the end monomers or A−B junction points. The evolution of the distribution of A−B junction points, $n_{A-B}(r)$, is shown in Figure 12a. At high salt concentration, when the pulling force exerted by the corona is not strong enough to provoke microphase segregation in the core, the distribution is rather narrow with a pronounced peak. Our calculations demonstrated that the distributions for ϕ_{ion}= 0.1 and 0.05 (the latter is not shown in Figure 12a) are indistinguishable, whereas the following decrease in ϕ_{ion} leads to broadening of the distribution and to progressive shift of the position of the maximum toward larger r. By analyzing the shape of the profiles, we can conclude that even though distributions are rather broad, each profile has one pronounced maximum, and we do not encounter the situation with two maxima corresponding to partitioning of the star arms into two groups, i.e., those whose B blocks are completely embedded in the core and those whose B blocks are (partially) expelled from the core and stretched. This finding justifies the used by the analytical theory approximation 1 that all the junction points were placed equidistantly from the center of the star.

The distribution of ends of corona blocks, Figure 12b, has one pronounced maximum. Upon a decrease in ϕ_{ion} that leads to an increase in the radius R of the A/B interface, the distribution becomes asymmetric, biased toward the edge of the star. Therefore, the use of assumption 2 is reasonable. Although, as it was noted above, in the one-gradient version of the SF-SCF method we cannot see the stretched "legs", they can be revealed by plotting the radial profiles of the number of B monomers per spherical layer. The $n_B(r)$ distribution allow us to analyze the local tension in the extended part of the core. Uniform "leg" stretching (according to assumption 5) would correspond to a plateau on the $n_B(z)$ profile. From Figure 13 we see that in our system this situation is better manifested in the case of very strong corona stretching force (very low ϕ_{ion}). Deviations from the flat plateau shape of the $n_B(z)$ profiles observed in Figure 13 (these deviations are also well seen in the plots of Figure 14) are due to the finite width of the distribution of the A−B junction points.

Radial distribution of a number of monomer units found at given distance from the center is also an appropriate characteristic for estimating the degree of overlap of the core and the corona (hence, we can test the validity of assumption 3). These profiles presented together on the same plot are shown in Figure 14 (the scale of the plot is chosen for better "zoom" of the A/B interfacial region). We see that $n_A(r)$ and $n_B(r)$ profiles (shown by black and gray lines, respectively) demonstrate a small overlap; the "maximum" value of the n_A and n_B in the overlap zone corresponds to intersection of the profile and is very close to the value of p (in our case p = 20). Hence, the fraction of monomers of "guest" A (B) component in the "host" B-core (A-coronal) domain is small, so we can conclude that the core and the corona are well segregated, even under the conditions of strong stretching of the inner B blocks; that is the case at low ϕ_{ion} values. By summing up the distributions presented in Figure 14, another interesting feature of the star with partially unfolded core is revealed. At strong corona pulling forces (low ionic strength), the distribution of the total number of monomer units, $n = n_A + n_B$, shown in Figure 15 has a plateau in the vicinity of the A/B boundary. This means that the strongly (and homogeneously) stretched "legs" include not solely the parts of B blocks extracted from the B core but also parts of A blocks adjoining the ends of the B blocks. The uniform stretching of the arms is typical for starlike polyelectrolyte in the "osmotic" (dominated by the counterions) regime. With an increase in r this plateau is followed by the growing part on $n(r)$ profile corresponding to the decrease in the local stretching of star arms which is typical for a convex

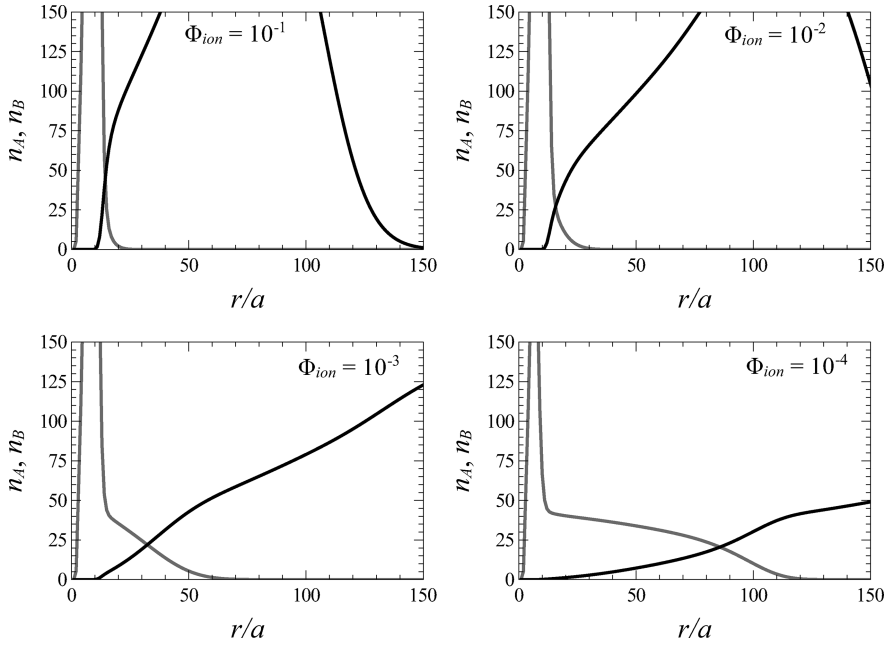

Figure 14. Radial distribution of the number of A (black curves) and B monomers (gray curves) in the vicinity of the A/B interface in AB core−shell star with $p = 20$, $N_A = 1000$, $N_B = 200$, $\chi_A = 0$, $\chi_B = 1$, $\alpha_b = 0.5$, and different values of ϕ_{ion} (shown in each panel).

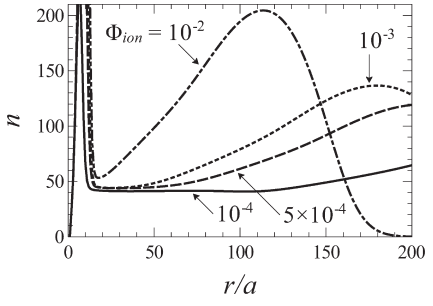

Figure 15. Radial distribution of total number of monomer units in AB core−shell star with $p = 20$, $N_A = 1000$, $N_B = 200$, $\chi_A = 0$, $\chi_B = 1$, $\alpha_b = 0.5$, and different values of ϕ_{ion} in the vicinity of the A/B interface.

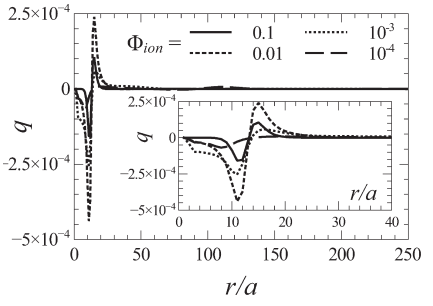

Figure 16. Radial distribution of local charge in AB core−shell star with $p = 20$, $N_A = 1000$, $N_B = 200$, $\chi_A = 0$, $\chi_B = 1$, $\alpha_b = 0.5$, and different values of ϕ_{ion}.

spherical (or cylindrical) polyelectrolyte brush in the salt-dominance regime.[13,35] At moderate and high ionic strength such a plateau is not observed.

Finally, to test the validity of the corona electroneutrality assumption 6, local charge density distribution $q(r) = \varphi_{Na^+}(r) + \alpha_b\varphi_A(r) - \varphi_{Cl^-}(r)$ was calculated. Figure 16 shows that in the corona the local charge density is perfectly zero; the distortions of local electroneutrality are observed at the A/B interface only.

CONCLUSIONS AND OUTLOOK

In the present paper, conformational transitions in an amphiphilic $(AB)_p$ block copolymer star with hydrophobic central blocks and polyelectrolyte terminal blocks were studied by means of analytical mean-field theory combined with the SF-SCF numerical modeling. The star is in aqueous media and forms under high ionic strength conditions a unimolecular micelle with collapsed B-core and extended A corona. Because of repulsive electrostatic interactions in the polyelectrolyte corona, the core is subjected to the radial extensional force. The strength of the interactions in the corona is governed by the degree of ionization of A blocks and by the ionic strength of the solution. From the experimental viewpoint, the salt concentration is the most common control parameter. We have shown that a decrease in the ionic strength of the solution may provoke the intramolecular conformational transition related to the unfolding of collapsed inner hydrophobic blocks. More specifically, the unimolecular $(AB)_p$ micelle undergoes two consecutive conformational transitions: The first one is continuous and is associated with the onset of the microphase segregation in the B core. The second one is the complete unfolding of the core which is accompanied by the jumpwise increases of the core size and the overall star size and the corresponding jumpwise decrease in the corona thickness. Remarkably, the second transition does not occur in the stars with sufficiently large number of arms. We have constructed the diagrams of states of $(AB)_p$ star in $\phi_{ion}-\alpha_b$ and $\phi_{ion}-p$ coordinates. The diagrams contain the region corresponding to unimolecular micelles with collapsed core, the region corresponding to the partial unfolded core-forming blocks, and, finally, the region corresponding to the conformation with

completely unfolded core and extended B blocks. The developed analytical theory is based on two essential approximations: The first one is the approximation of local electroneutrality of the corona. Both analytical and numerical Poisson−Boltzmann analysis convincingly prove[28] that for a reasonable degree of ionization ($\alpha_b \geq 0.1$) the approximation is very accurate for the stars with the number of arms $p \geq 10$. The second one is the equal arm stretching approximation. The latter is well-justified for the unimolecular micelles with collapsed B-core as well as for the conformations with completely unfolded core.[28] The situation, however, is more delicate in the regime with phase segregated (partially unfolded) core. In particular, one could expect that there is an analogy to the collapse transition in hydrophobic polyelectrolyte stars and brushes: Theories based on the equal stretching approximation[29−31] predicted a jump-wise "unfolding" transition. On the other hand, more accurate approaches[32,33] pointed to the coexistence of two populations of chains (collapsed and stretched) and smooth variation of the average dimensions in the transition range due to progressive repartitioning of the chains between the collapsed and the extended states. Therefore, we have complemented our analytical theory of the unfolding transition in the $(AB)_p$ block copolymer stars by numerical calculations made with the aid of assumption-free SF-SCF method. The results of the SCF modeling have confirmed the predicted scenario of the core unfolding in the amphiphilic $(AB)_p$ star and shown that, with an increase in electrostatic repulsions in the corona, the core unfolding occurs via microphase segregated states. Importantly, the SCF calculations have proven that at any ionic strength (i.e., both in the microphase-segregated and in the unfolded conformations) the end segments of the A-blocks and the A−B junction points exhibit unimodal radial distributions, each with a single maximum. This observation proves that the analytical theory based on the equal stretching approximation gives a qualitatively correct (artifact-free) description of the conformations and intramolecular unfolding transition in amphiphilic $(AB)_p$ star.

In the present paper we considered $(AB)_p$ star copolymers with a quenched fraction of permanently charged monomer units in the A block. Correspondingly, the ionic strength of the solution was chosen as a control parameter, variation in which triggers the intramolecular conformational transitions. In the case of the copolymers comprising weakly dissociating (pH-sensitive) polyelectrolyte blocks, the degree of ionization, and, as a result, the conformation of the copolymer can be affected by variation in pH as well. Moreover, in the case of branched polyelectrolytes the degree of ionization of branches is not controlled solely by the value of pH in the buffer but depends also on the ionic strength of the solution and on the polymer conformation. This coupling causes highly nontrivial responsive behavior of the pH-sensitive branched (co)polymers. In particular, continuous variation in the ionic strength at pH $\approx$ pK may cause re-entrant folding−unfolding transition. These effects will be addressed in the forthcoming publication.

Above we have considered very dilute solutions of $(AB)_p$ star copolymers which form spherical unimolecular micelles. At higher concentrations, the aggregation of $(AB)_p$ unimolecular micelles with small number of arms may lead to formation of intermolecular assemblies. Depending on the lengths of the hydrophobic and polyelectrolyte blocks this aggregation may give rise not only to spherical but also to cylindrical micelles, lamellar, or bicontinuous structure.[34] For amphiphilic ionic/hydrophobic diblock copolymers, the morphology of the intermolecular aggregates is controlled by the length of the A and B blocks; the morphological transitions can be triggered by variation in the ionic strength or in pH. The connectivity of the amphiphilic block copolymers into stars introduces additional topological constraints which may influence the morphologies of the intermolecular assemblies of $(AB)_p$ stars as compared to those formed by homologous diblock copolymers ("single arms"). We remark, however, that because of strong steric repulsions between polyelectrolyte coronae of the unimolecular micelles, their aggregation may be significantly hindered kinetically. Analysis of the intermolecular assembly of the $(AB)_p$ star copolymers is, however, beyond the scope of the present work.

AUTHOR INFORMATION

Corresponding Author
*E-mail: oleg.borisov@univ-pau.fr.

ACKNOWLEDGMENT

The authors are thankful to Professor F. A. M. Leermakers for introduction to the SF-SCF approach and sharing software package SFBox. Financial support by the Russian Foundation for Basic Research (RFBR) through Project 11-03-00969-a, by the Department of Chemistry and Material Science of the Russian Academy of Sciences, by the funds from the EC Sixth Framework Program through the Marie Curie Research and Training Network POLYAMPHI, and by the Scientific and Technological Cooperation Program Switzerland−Russia, project "Experimental studies and theoretical modeling of amphiphilic di/triblock and dendritic functional polymers at surfaces: influence of interfacial architecture on biological response", Grant Agreement No. 128308, is gratefully acknowledged.

REFERENCES

(1) Riess, G. *Prog. Polym. Sci.* **2003**, *28*, 1107–1170.
(2) Kataoka, K.; Harada, A.; Nagasaki, Y. *Adv. Drug Delivery Rev.* **2001**, *47*, 113.
(3) Gillies, E. R.; Fréchet, M. J. *Pure Appl. Chem.* **2004**, *76*, 1295.
(4) Haag, R. *Angew. Chem., Int. Ed.* **2004**, *43*, 278–282.
(5) Alberts, B.; Johnson, A.; Lewis, J.; Raff, M.; Roberts, K.; Walter, P. *Molecular Biology of the Cell*; Garland Publishing: New York, 2002.
(6) Fustin, C.-A.; Abetz, V.; Gohy, J.-F. *Eur. Phys. J. E* **2005**, *16*, 291–302.
(7) Filali, M.; Meier, M. A. R.; Schubert, U. S.; Gohy, J.-F. *Langmuir* **2005**, *21*, 7995–8000.
(8) Zhang, L.; Niu, H.; Chen, Y.; Liu, H.; Gao, M. *J. Colloid Interface Sci.* **2005**, *298*, 177–182.
(9) Daoud, M.; Cotton, J.-P. *J. Phys. (Paris)* **1982**, *43*, 531–538.
(10) Zhulina, E. B. *Polym. Sci. USSR* **1984**, *26*, 794–798.
(11) Zhulina, E. B. *Polym. Sci. USSR* **1984**, *26*, 834–838.
(12) Birshtein, T. M.; Zhulina, E. B. *Polymer* **1984**, *25*, 1453–1461.
(13) Zhulina, E. B.; Birshtein, T. M.; Borisov, O. V. *Eur. Phys. J. E* **2006**, *20*, 243–256.
(14) Alexander, S. *J. Phys. (Paris)* **1977**, *38*, 983–987.
(15) de Gennes, P.-G. *Macromolecules* **1980**, *13*, 1069–1075.
(16) Zhulina, E. B.; Borisov, O. V.; Birshtein, T. M. *Polym. Sci. USSR* **1988**, *30*, 780–788.
(17) Mercurieva, A. A.; Birshtein, T. M.; Leermakers, F. A. M. *Langmuir* **2009**, *25*, 11516–11527.
(18) Nelson, P. H.; Rutledge, G. C.; Hatton, T. A. *Comput. Theor. Polym. Sci.* **1998**, *8*, 31–38.
(19) Williams, D. R. M. *J. Phys. II* **1993**, *3*, 1313.

(20) Halperin, A.; Zhulina, E. B. *Europhys. Lett.* **1991**, *15*, 417.
(21) Halperin, A.; Zhulina, E. B. *Macromolecules* **1991**, *24*, 5393–5397.
(22) Polotsky, A. A.; Charlaganov, M. I.; Leermakers, F. A. M.; Daoud, M.; Borisov, O.; Birshtein, T. M. *Macromolecules* **2009**, *42*, 5360–5371.
(23) Polotsky, A. A.; Daoud, M.; Borisov, O.; Birshtein, T. M. *Macromolecules* **2010**, *43*, 1629–1643.
(24) Cooke, R.; Williams, D. R. M. *Europhys. Lett.* **2003**, *64*, 267–273.
(25) Ushakova, A. S.; Govorun, E. N.; Khokhlov, A. R. *J. Phys.: Condens. Matter* **2006**, *18*, 915–930.
(26) de Gennes, P.-G. *Scaling Concepts in Polymer Physics*; Cornell University Press: Ithaca, NY, 1979.
(27) Fleer, G. J.; Cohen Stuart, M. A.; Scheutjens, J. M. H. M.; Cosgrove, T.; Vincent, B. *Polymers at Interfaces*; Chapman and Hall: London, 1993.
(28) Borisov, O. V.; Zhulina, E. B.; Leermakers, F. A. M.; Müller, A. H. E.; Ballauff, M. *Adv. Polym. Sci.* **2011**, *241*, 1–55.
(29) Borisov, O. V.; Birshtein, T. M.; Zhulina, E. B. *J. Phys. II* **1991**, *1*, 521.
(30) Borisov, O. V.; Birshtein, T. M.; Zhulina, E. B. *Prog. Colloid Polym. Sci.* **1992**, *90*, 177.
(31) Ross, R.; Pincus, P. *Macromolecules* **1992**, *25*, 2177–218.
(32) Misra, S.; Mattice, W. L.; Napper, D. H. *Macromolecules* **1994**, *27*, 7090–7098.
(33) Pryamitsyn, V. A.; Leermakers, F. A. M.; Fleer, G. J.; Zhulina, E. B. *Macromolecules* **1996**, *29*, 8260–8270.
(34) Strandman, S.; Zarembo, A.; Darinskii, A. A.; Löflund, L.; Butcher, S. J.; Tenhu, H. *Polymer* **2007**, *48*, 7008–7016.
(35) Birshtein, T. M.; Mercurieva, A. A.; Leermakers, F. A.; Rud, O. V. *Polym. Sci. Ser. A (Russia)* **2008**, *50*, 992–1007.